# First-in-human evaluation of cutaneous innate and adaptive immunomodulation by mosquito bites

David Guerrero[1,*], Hoa Thi My Vo[1,*], Chanthap Lon[3,*], Jennifer A. Bohl[2], Sreynik Nhik[3], Sophana Chea[3], Somnang Man[3,4], Sokunthea Sreng[3,4], Andrea R. Pacheco[3], Sokna Ly[3], Rathanak Sath[3], Sokchea Lay[1], Dorothee Missé[5], Rekol Huy[4], Rithea Leang[4], Hok Kry[6], Jesus G. Valenzuela[2], Fabiano Oliveira[2,$],Tineke Cantaert[1,$], Jessica E. Manning[2,3,$,#]

[1] Institut Pasteur du Cambodge, Pasteur Network, Phnom Penh, Cambodia

[2] Laboratory of Malaria and Vector Research, National Institute of Allergy and Infectious Diseases, National Institutes of Health, Rockville, Maryland, USA

[3] International Center of Excellence in Research, National Institute of Allergy and Infectious Diseases, National Institutes of Health, Phnom Penh, Cambodia

[4] National Center of Parasitology, Entomology, and Malaria Control, Phnom Penh, Cambodia

[5] MIVEGEC, Univ Montpellier, IRD, CNRS, 34000 Montpellier, France.

[6] Kampong Speu Provincial District, Ministry of Health, Phnom Penh, Cambodia

*co-first author

$ co-last author

# corresponding author: jessica.manning@nih.gov

**Abstract**

Mosquito-borne viruses are a growing global threat. Initial viral inoculation occurs in the skin via the mosquito 'bite', eliciting immune responses that shape the establishment of infection and pathogenesis. We aimed to cutaneous innate and adaptive immune responses to mosquito bites in individuals from endemic areas. In this single-arm, cross-sectional interventional study, we enrolled 30 healthy adult participants aged 18 to 45 years of age from Cambodia between October 2020 and January 2021. We performed 3-mm skin biopsies at baseline as well as 30 minutes, 4 hours, and 48 hours after a controlled feeding by uninfected *Aedes aegypti* mosquitos. The primary endpoints were measurement of changes in early and late innate responses in bitten vs unbitten skin by gene expression profiling, immunophenotyping, and cytokine profiling. Results revealed induction of neutrophil degranulation and recruitment of skin-resident dendritic cells and M2-macrophages in 'bitten' skin. As the immune reaction progressed over time, T cell priming and regulatory pathways were upregulated along with a shift to a Th2-driven response and CD8+ T cell activation. In accordance, participants' bitten skin cells produced less pro-inflammatory cytokines when stimulated by *Ae. aegypti* salivary gland extract. No unexpected adverse events occurred, and one patient was lost to follow-up at Day 14. These results identify key immune genes, cell types, and pathways in the human response to mosquito bites that can be leveraged to develop novel therapeutics and vector-targeted vaccine candidates to arboviral diseases.

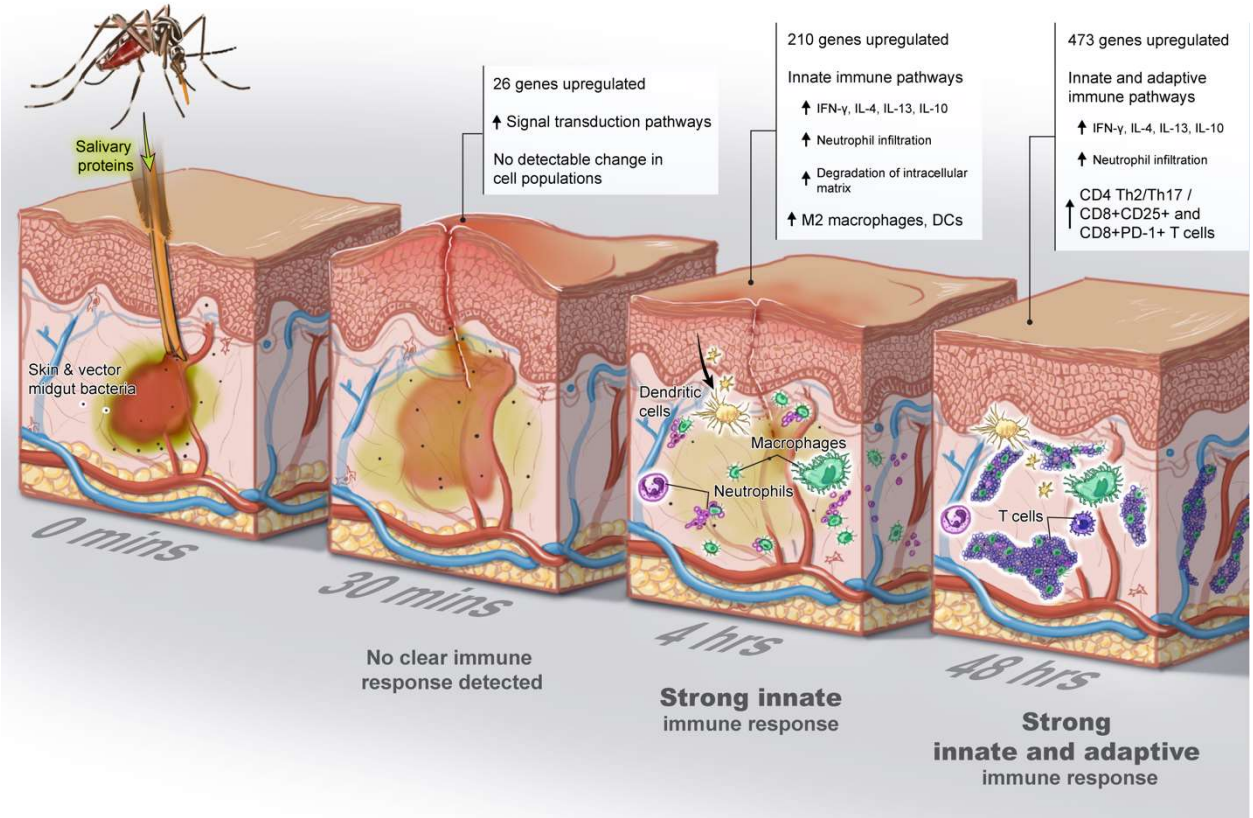


**Graphical Abstract**

**Panel shows evolution of the human skin response to *Aedes aegypti* bites over time.**

61 **Introduction**

62 With one million deaths every year, vector-borne diseases remain a major health problem
63 worldwide[1]. In particular, arboviruses are of particular concern given a global distribution and a
64 burden of nearly half a billion infections[2]. Several clinically significant arboviruses such as yellow
65 fever (YFV), dengue (DENV), chikungunya (CHIKV), and Zika (ZIKV) viruses are all transmitted
66 by *Aedes spp*. mosquitoes. These vectors are abundant in tropical and subtropical areas, but current
67 climate change and rapid urbanization are expanding their transmission potential and increasing
68 the at-risk population[3].

69 Mosquitoes first acquire an arbovirus via insertion of their proboscis into the dermis of an infected
70 host during a blood meal. The virus then replicates in midgut cells to later disseminate and reach
71 the salivary glands (SG)[4]. During a subsequent blood meal, the infectious mosquito inoculates
72 virus and insect-derived molecules, including salivary components, into the dermis of a new
73 human host. The saliva from hematophagous mosquitoes is a cocktail of pharmacologically active
74 molecules, some of which are anti-hemostatic, angiogenic, and immunomodulatory[5–7]. Over the
75 last couple decades, several animal and *in vitro* studies demonstrated that inoculation of vector
76 saliva, and/or concomitant blood-feeding by an arthropod, can immunomodulate the host antiviral
77 response in the skin and periphery[7–10]. These perturbations result in altered cytokine production
78 profiles [11–13], promotion of recruitment of infection-susceptible cells to the bite site[14,15], stimulation
79 of autophagy activation[5], and an induction of neutrophil infiltration to the local inflammation site[15]
80 amongst other consequences. Mosquito-inoculated DENV or ZIKV infection in macaques led to
81 higher or delayed viremia compared to non-vector or needle inoculation routes[16,17]. With regard to
82 clinical pathogenesis, mice inoculated with both Semliki Forest virus and mosquito saliva had
83 higher loads of virus RNA in the skin, earlier brain dissemination, and more frequent lethal

84 outcomes than animals inoculated with virus alone[12]. Taken together, arthropod-mediated viral
85 infection leads to increased disease progression, viremia, and mortality[8,9]. Despite this robust
86 evidence from animal and *in vitro* studies, there are no translational studies on the human skin
87 response to mosquito bites, much less those in tropical areas. Individuals are continuously exposed
88 to mosquito bites, possibly shaping their immune responses to mosquito salivary proteins in
89 contrast to those intermittently or rarely exposed[18,19]. In order to examine the dermal and epidermal
90 innate and adaptive immune responses to *Ae. aegypti* saliva, we compared the immune responses
91 before and after *Ae. aegypti* bites in skin biopsies from 30 healthy Cambodian individuals living
92 in an area where *Ae. Aegypti* mosquitoes are prevalent. Our study provides information on the key
93 genes and cell populations involved in the human immune response at different time points after
94 the 'mosquito bite.'

95 **Results**

96 **Controlled *Aedes aegypti* bite challenge in healthy volunteers in Cambodia**

97 From October 2020 to January 2021, we enrolled 30 healthy Cambodian adults at Kampong Speu
98 District Referral Hospital in Chbar Mon, Cambodia. The study population comprised 13 females
99 and 17 males, all of whom were of Khmer (Cambodian) ethnicity (Supplementary Table 1). The
100 population was randomly divided in three groups to assess immune responses by different
101 technologies (Fig. 1). The median age was 32.5 years (IQR 22–35) and the primary occupations
102 were variable, although nearly half (14/30) were unemployed. In terms of mosquito exposure risk,
103 most participants reported living in a house (20/30), being middle income (25/30), having one to
104 two domestic water containers (22/30). Notably, most participants did not use larvicide (28/30) or
105 insecticide (19/30) in their homes. Only 10% (3/30) reported prior dengue infection, but all 30
106 participants were positive for dengue anti-NS1 antibodies. All participants had detectable IgG to

107 *Ae. aegypti* salivary gland extract (SGE) prior to mosquito feeding, and these levels were not
108 significantly different by age, gender, or 14 days after the mosquito feeding (Supplementary Figure
109 S1). One participant did not complete Day 14 follow-up and was considered lost to follow-up.
110 No unanticipated adverse events occurred with the biopsies or mosquito feedings.

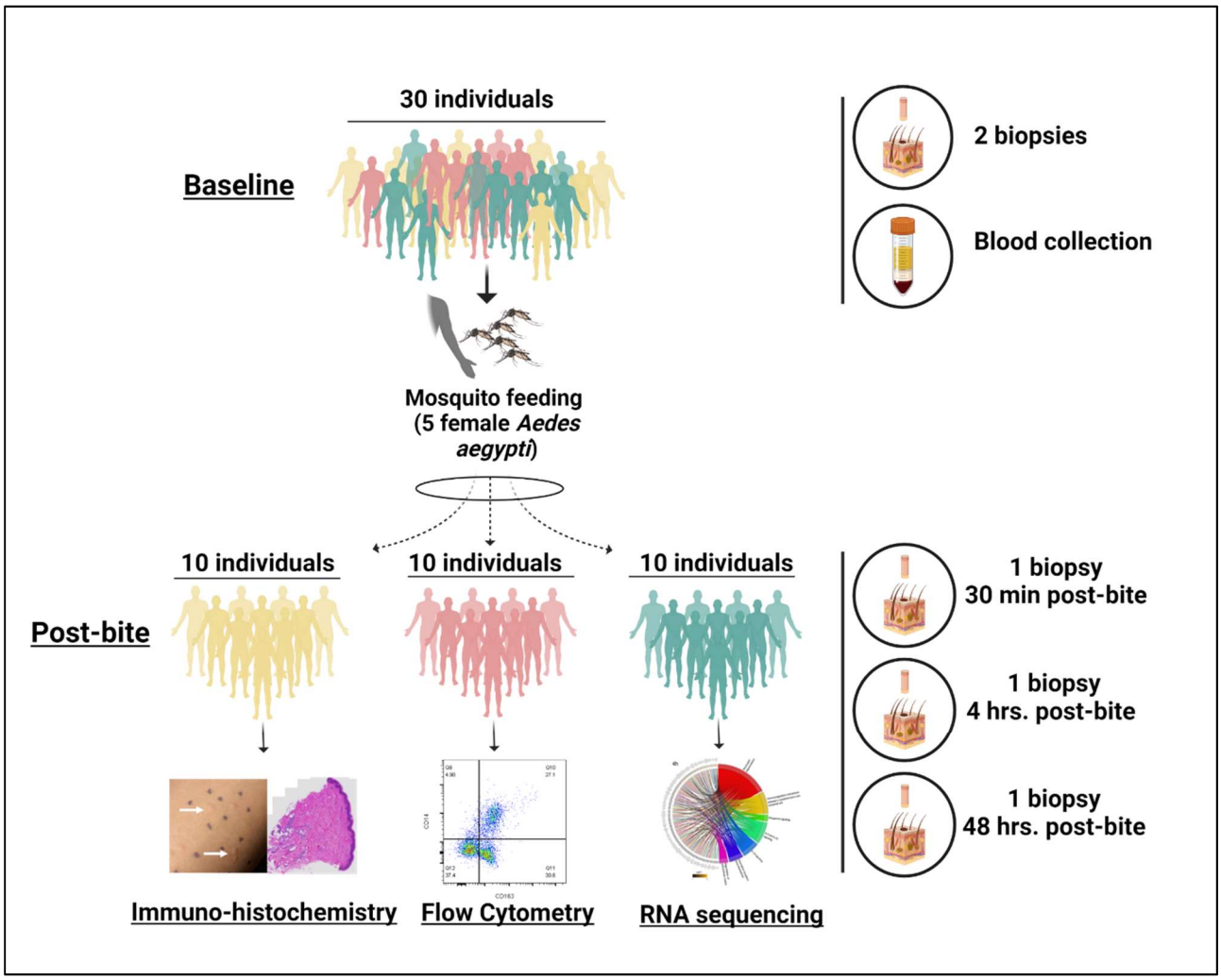


111

112 Figure 1. **Graphical Representation of Study Design.** Thirty Cambodian participants were
113 enrolled in the study. Each patient underwent a mosquito feeding (5 females *Aedes aegypti*) for
114 ten minutes. Each volunteer underwent a 3mm biopsy from a mosquito bite site at 30 minutes, 4
115 hours, and 48 hours. Distinct bite sites were biopsied at different time points. Additionally, two

116 3mm biopsies of normal skin (NSK) were taken from the opposite forearm. Blood was collected
117 to obtain serum.

118 **Marked clinical changes occurred in the skin post-mosquito feeding**

119 Exposure to five *Ae. aegypti* mosquitos resulted in 3 to 10 visible bite sites per volunteer. Upon
120 clinical observation, participants experienced erythema and swelling with a "bite size" reaction
121 that peaked at 15 minutes after feeding (Fig. 2a). The mean bite size of 4.9mm at 15 min after
122 feeding decreased to 4.7 mm at 30 minutes, to 2.7 mm at 4 hours and gradually decreased to 2.1mm
123 by 48 hours (Supplementary Table 1). Observation of representative histological sections shows
124 increased recruitment of cells to the dermis and epidermis at 48 hours post-bite (Fig. 2b,c). There
125 was no difference in bite size reaction by gender or age.

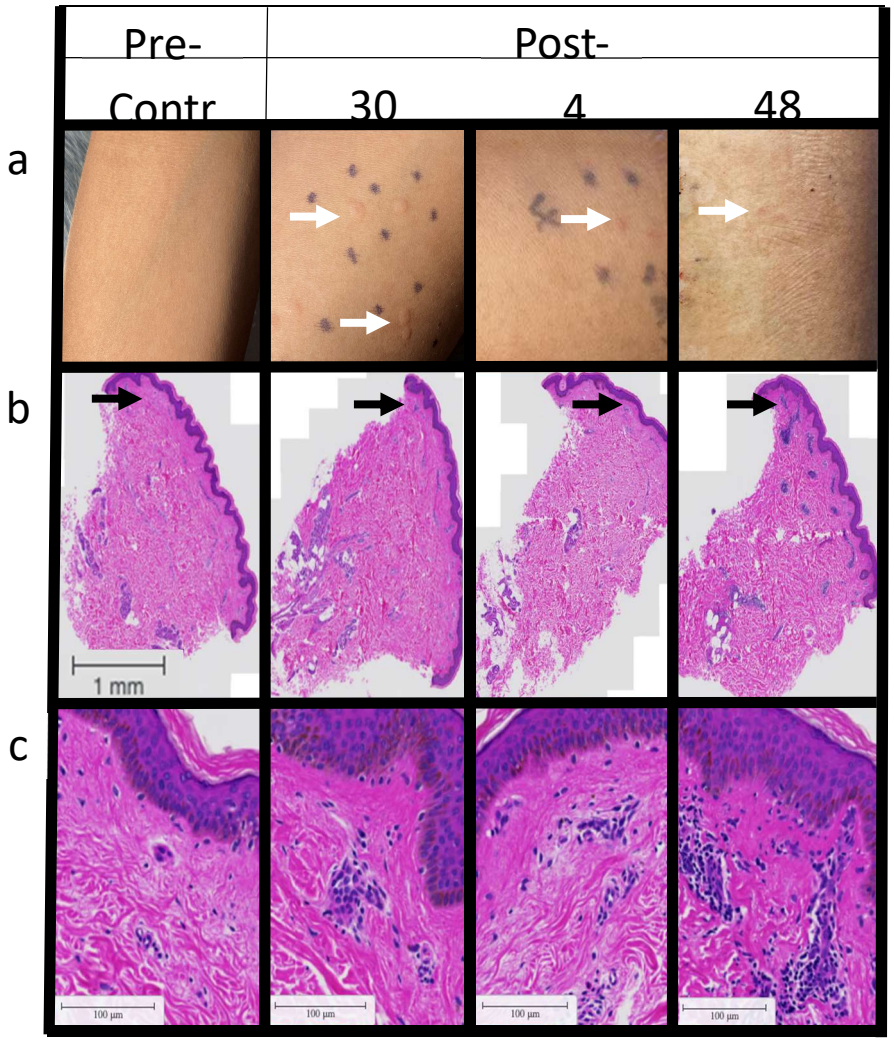


Figure 2. **Clinical observations of skin reaction pre- and post-bite on gross examination and H&E staining. a,** Skin immune responses to mosquito bites (left to right) normal skin (NSK), 30 minutes, 4 hours, and 48 hours after exposure to five *Ae. aegypti* mosquitos. **b,** Representative cross-sectional of 3mm punch biopsies H&E stained at (left to right) 0 hours, 30 minutes, 4 hours, and 48 hours after exposure to *Ae. aegypti* bites. Distinct bite sites were biopsied at different time points. Scale bar is 1 mm. Black arrows indicate area of infiltrate. **c,** Magnification of infiltrate indicated by black areas in B, scale bar 100µM.

135 **Changes in gene expression in *Aedes aegypti* bitten versus normal skin (NSK) evolved over**
136 **48 hours**

137 We extracted RNA and performed next generation sequencing on 40 skin biopsies from 10
138 participants (baseline normal skin (NSK) biopsy on the forearm, plus 3 follow-up biopsies each at
139 30 minutes, 4 hours, and 48 hours post *Ae. aegypti* bites on the contralateral arm). Principal
140 Component (PC) analysis of *Ae. aegypti* bite site skin biopsies resulted in segregation of sample
141 clusters based on the time the biopsy was taken (Fig. 3a), with PC1 and PC2 variances defining
142 differences between NSK and 30 minutes versus 4 hours and 48 hours. While PC3 variance
143 associated to the separation between biopsies taken at 4 hours and 48 hours, samples taken from
144 NSK (pink circles) and 30 minutes after *Ae. aegypti* bites clustered in the same spatial area. At 4
145 hours post-bite, 6 of 10 samples occupied a distinct region (Fig. 3a, blue ellipse) from NSK, 30
146 minutes or 48 hours after *Ae. aegypti* bites. Similarly at 48 hours post-bite, 7 of 10 samples
147 segregated into a discrete space (Fig. 3a, orange ellipse) compared to NSK, 30 minutes or 4 hours
148 after *Ae. aegypti* bites. These data indicate that time post-bite rather than inter-individual
149 differences drive unique patterns in gene expression. Differential analysis of RNA expression with
150 a threshold of two-fold ($-1 < \log2FC > 1$; False discovery rate (FDR) $< 0.05$) over NSK biopsies
151 resulted in 709 upregulated genes post-bite compared to 31 downregulated genes (Fig. 3b, red
152 circles). At 30 minutes, 4 hours, and 48 hours after a mosquito bite, 26, 210 and 473 genes were
153 upregulated over NSK, respectively (Fig. 3c, Supplementary Table 2). Conversely, one gene at 4
154 hours and 27 genes at 48 hours were downregulated after *Ae. aegypti* bites (Supplementary Table
155 2).

156 Upregulated genes at each time point were subjected to over-representation analysis (ORA) for
157 enriched pathways using the Reactome database with an FDR cut off $< 0.05$. Four pathways related

158 to cell proliferation, cell growth and nuclear transcription were identified (FDR < 0.05) at 30
159 minutes after *Ae. aegypti* bites (Supplementary Table 3). At both 4 and 48 hours post-bite, the
160 immune nature of the host response to *Ae. aegypti* bites was evident via the revealed pathways
161 (Fig. 3d, Supplementary Table 3). At 4 hours post-bite, pathways such as "neutrophil
162 degranulation", "Interleukin-4 and Interleukin-13 signaling", "Interleukin-10 signaling",
163 "Interferon-γ signaling" "Chemokine receptors bind chemokines" and "Immunoregulatory
164 interactions between a Lymphoid and a non-Lymphoid cell" (Fig. 3d, upper chord) were
165 significantly overrepresented and maintained until 48 hours post-bite (Fig. 3d, lower chord).
166 Unique pathways discovered at 4 hours post-bite were related to "degradation of extracellular
167 matrix" (Fig 3d, upper chord) while "antimicrobial peptides" pathway and "adaptive immune
168 system processes" were present at 48 hours post-bite including "TCR signaling", "Co-stimulation
169 by the CD28 family", "PD-1 signaling", "MHC class II antigen presentation" (Fig. 3d, lower
170 chord). A heatmap with differentially expressed genes (DEG) under an FDR cutoff < 0.05 and
171 log2FC >1 in at least one timepoint was assembled (Supplementary Figure S2, Supplementary
172 Table 4), showing the dynamics of DE expression throughout the three timepoints. Fig. 3e shows
173 DEG driving the common pathways found on Fig. 3d.

174 Overall, few DEG genes were detected at 30 minutes post-bite compared to NSK biopsies. The
175 main upregulated gene FOSB (up 18.8x) is one of the transcription factors of the FOS family
176 proteins that regulate cell proliferation and differentiation (Supplementary Table 2). As the
177 reaction progresses over time, gene expression increased towards neutrophil recruitment followed
178 by signaling of both Th1, Th2, and regulatory pathways. The five most regulated genes at 4 hours
179 compared to NSK are KRT6C (related to keratinization; up 80.8x), CXCL8 (neutrophil-attracting
180 chemokine IL-8 up 75.0x), TNIP3 (inhibitor of NF-kappa-B activation; up 59.3x), IL-20

181 (stimulates keratinocyte proliferation and differentiation; up 59.1x) and IL-1B (pro-inflammatory
182 cytokine; up 45.7x) (Supplementary Table 2). The immune response evolved at 48 hours post-bite
183 to include adaptive immune response pathways related to T-cell priming. The five top genes at 48
184 hours are KRT6C (related to keratinization; up 59.6x), DEFB4A (an antimicrobial peptide; up
185 32.7x), GZMB (Granzyme B, up 21.1x), TCL1A (proliferation of T and B cells; up 20.3x) and
186 CCL18 (chemokine associated with associated with TH2 responses; up 18.5x).

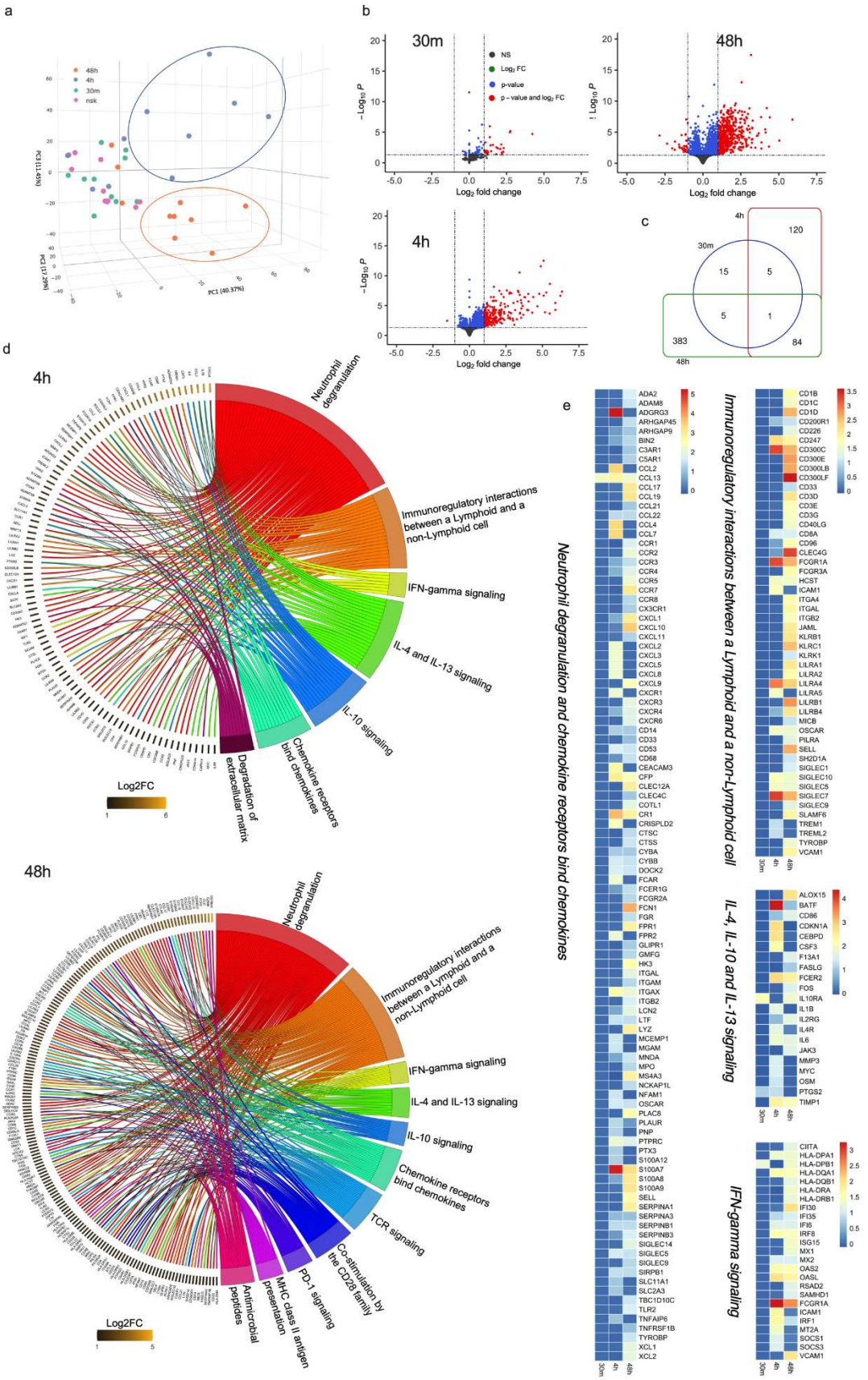
a
48h
4h
30m
nsk
PC1 (40.37%)
PC2 (17.26%)
PC3 (11.43%)
b
30m
48h
4h
NS
Log2 FC
p-value
p – value and log2 FC
– Log10 P
Log2 fold change
c
4h
30m
48h
120
15
5
5
1
383
84
d
4h
48h
Neutrophil degranulation
Immunoregulatory interactions between a Lymphoid and a non-Lymphoid cell
IFN-gamma signaling
IL-4 and IL-13 signaling
IL-10 signaling
Chemokine receptors bind chemokines
TCR signaling
Co-stimulation by the CD28 family
PD-1 signaling
MHC class II antigen presentation
Antimicrobial peptides
Degradation of extracellular matrix
Log2FC
e
Neutrophil degranulation and chemokine receptors bind chemokines
Immunoregulatory interactions between a Lymphoid and a non-Lymphoid cell
IL-4, IL-10 and IL-13 signaling
IFN-gamma signaling
30m
4h
48h

188 Figure 3. **Differential expression gene (DEG) and pathway analysis induced by *Aedes aegypti***
189 **mosquito bites over time. a,** 3D principal component analysis showing clustering of individual
190 biopsies taken at 30 minutes (green dots), 4 hours (blue dots), 48 hours (orange dots) post-bite or
191 normal skin (NSK; pink dots). Blue ellipse indicates clustering at 4 hours, while orange ellipse at
192 48 hours. **b,** Volcano plot comparing DEG from skin biopsies post-bite with NSK (significant
193 genes with $-1 < \log2FC > 1$ and $FDR < 0.05$ are shown in red). **c,** Venn diagram summarizing the
194 relationships between significantly upregulated genes over NSK ($\log2FC > 1$ and $FDR < 0.05$) and
195 time post-bite. **d,** Chord plot shows significantly upregulated genes at 4 hours and 48 hours post-
196 bite over NSK (left side of chord plot) and overrepresented pathways (right side of chord plot).
197 Outer left ring shows genes and color range displays log2 fold change (left, key at bottom) or
198 Reactome terms (outer right ring). Chords connect gene names with Reactome term pathways. **e,**
199 Heatmap (scaled to log2FC) displaying a list of DEGs based on the common pathways
200 overrepresented at 4- and 48-hours post-bite.

201

202 **Early innate immune response in the skin is characterized by increased proportions of DCs**
203 **and M2 macrophages and a decreased proportion of NK cells**

204 To confirm and extend the gene expression analysis, dissociated cells from NSK and skin biopsies
205 taken at 30 minutes and 4 hours after exposure to mosquitos, were characterized for innate and
206 adaptive immune subsets by flow cytometry (Supplementary Figure S3, Supplementary Table 5).
207 No significant changes in cell populations were detected between NSK and 30 minutes post-bite,
208 mirroring the transcriptomic analysis of DEG. At 4 hours post-bite, the proportion of dendritic
209 cells (DC), and M2 macrophages increased, while the proportion of mast cells, natural killer (NK)
210 and T-cells decreased, when compared to NSK and 30 minutes post-bite (Fig. 4a). The frequencies

211 of DC subsets increased at 4 hours post-bite compared to NSK and 30 minutes (Fig. 4 b-e). Within
212 the DC subsets, Langerhans cells (CD45+CD3-CD207+) increased at 4 hours compared to NSK
213 (Fig. 4d). A decreasing, though non-significant trend in the NK cell population frequency was
214 observed over time (Fig. 4f). Regarding the macrophage population, M2-skewed macrophages
215 (CD45+CD14+CD163+) frequency increased after 4 hours post-bite as well as their expression of
216 activation markers (CD16/CD69) compared to NSK and 30 minutes (Fig. 4 h-j). Frequencies of
217 activated M2 macrophages, and frequency of Langerhans cells positively correlated with clinically
218 observed changes in bite size at 30 minutes (Supplementary Figure S4 a, b). In order to evaluate if
219 changes in total leukocytes ($CD45^+$) were affecting the reported frequencies, we analysed the
220 changes of the innate cell population within total live cells. Here, similar results were observed
221 (Supplementary Figure S5). Unfortunately, we did not include specific neutrophil markers to our
222 flow cytometry panels. Alternatively, when we gated on CD45+CD11b+CD14-CD56-CD117-
223 cells, that comprises mostly of neutrophils, we detect a significant "neutrophils" accumulation at
224 4 hours post-bite compared to NSK (Supplementary Figure S6). The relative proportion of $CD4^+$
225 and $CD8^+$ T cells did not change over time. Taken together, the results suggest that immune cell
226 infiltration and migration occurs in local skin tissue within 4 hours post-bite and is characterized
227 by increased frequencies of DCs, M2 macrophages and neutrophils, but decreased frequencies of
228 NK cells.

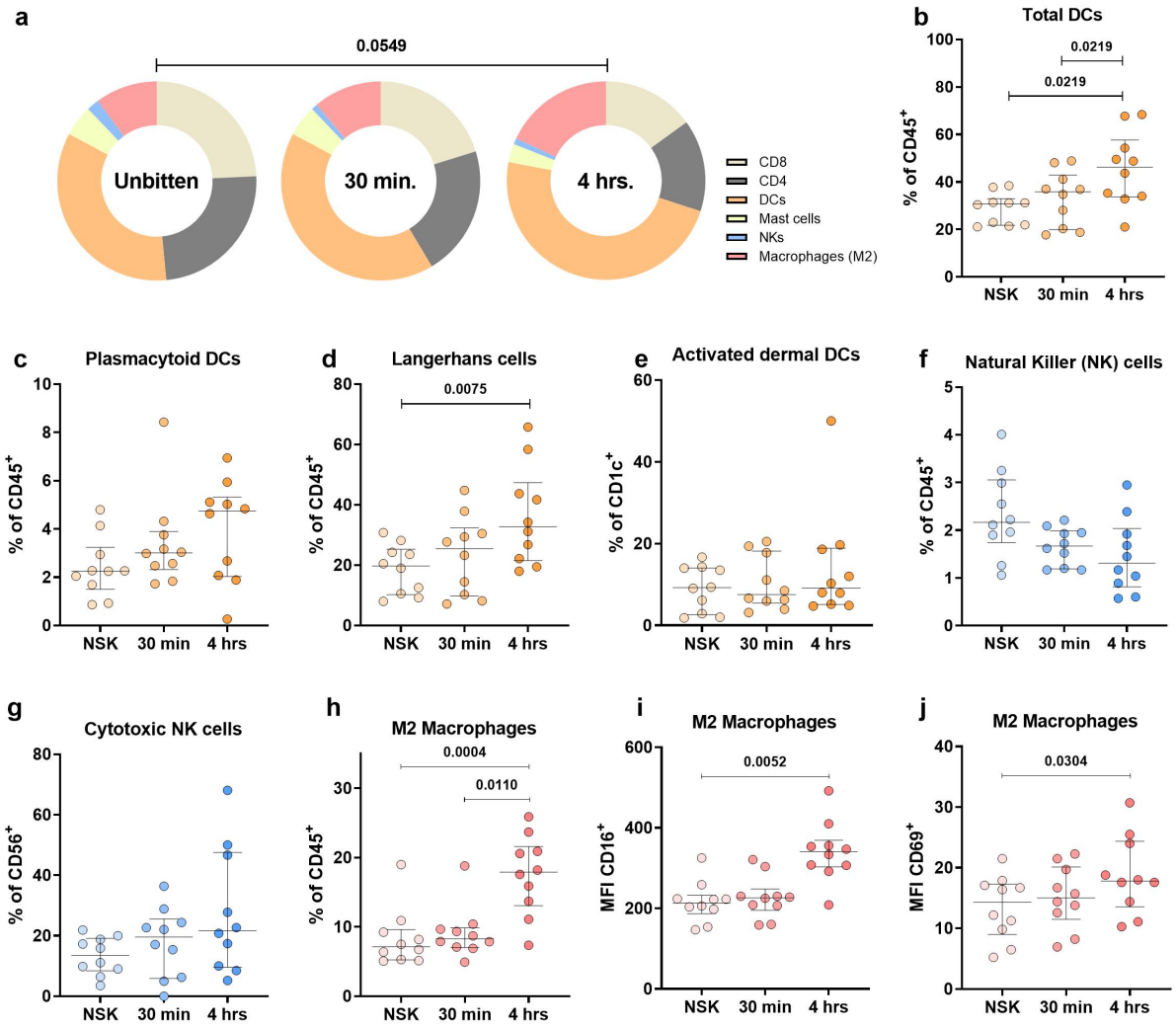


229

230 Figure 4. **Early innate immune responses in the skin are characterized by increased**
231 **proportions of DCs and M2 macrophages, and a decreased proportion of NK cells at 4 hours**
232 **post-bite**. **a,** Pie charts showing changes in the frequencies of skin immune cells during early
233 innate immune response to mosquito bite at 30 minutes and 4 hours after exposure. Frequencies
234 are reported as percentages of total leukocytes ($CD45^+$) **b,** total frequency of dendritic cells
235 calculated as the sum of Langerhans ($CD207^+$), dermal ($CD1c^+$) and plasmacytoid ($CD123^+$) DCs.
236 **c,d,** Frequency of plasmacytoid dendritic cells and Langerhans cells populations reported as
237 percentage of total $CD45^+$ cells shows significant increase of the later, at 4 hours post mosquito

238 bites. **e,** Frequency of activated dermal DCs ($CD1c^{+}CD69^{+}$) from the total dermal DCs population
239 ($CD1^{+}$). **f,** Frequency of NK cells (CD56) reported as percentage of total CD45+ cells. **g,**
240 Frequency of cytotoxic NK cells (CD56+CD16+) as percentage of total NK cells. **h-j**, Frequency
241 of M2 macrophages and MFI of their expressed activation markers CD16 and CD69. Statistical
242 analysis were performed with Chi-square test (**a)** and Friedman + Dunn's multiple comparisons
243 test (**b-j**). Bars indicate median and interquartile range. N=10

244

245 **Changes in the T cell compartment are observable at 48 hours after mosquito 'bite'**

246 Changes in skin T cell populations were assessed using NSK and biopsies taken at 48 hours post-
247 bite. We found that the frequency of CD8+CD25+ and CD8+PD-1+ T-cells increased at 48 hours
248 post-bite, compared to the NSK (Fig. 5a). Frequencies of CD8+ T cells correlated inversely with
249 the bite size at 48 hours (Supplementary Figure S4c). The frequency of effector memory cells re-
250 expressing CD45RA ($T_{EMRA}$) CD8 T cells (CD8+CCR7-CD45RA+) decreased at 48 hours (Fig.
251 5b). In the CD4+ T cell compartment, we observed a decrease in the frequency of Th1/Th17
252 (CD4+CCR4-CXCR3+) cells at 48h compared to NSK and an increase in the frequency of
253 Th2/Th17 (CD4+CCR4+CXCR3-) cells (Fig. 5c). The frequency of CD4+ effector memory T
254 cells ($T_{EM}$) (CD4+CCR7-CD45RA-) increased at 48 hours compared to NSK, while the frequency
255 of $T_{EMRA}$ cells (CD4+CCR7-CD45RA+) decreased (Fig. 5d). Results were similar when analyzing
256 the changes of T cell frequencies within all live cells (Supplementary Figure S7). Interestingly,
257 no changes were observed in the frequencies of skin-resident CD4 (CD4+CD103+CLA+) or CD8
258 (CD8+CD103+CLA+) T cells (Supplementary Figure S8). At 48 hours post-bite, these results
259 show an increase in the frequency of activated CD8 T cells in addition to a shift from Th1/Th17
260 towards Th2/Th17 polarization of CD4 T cells.

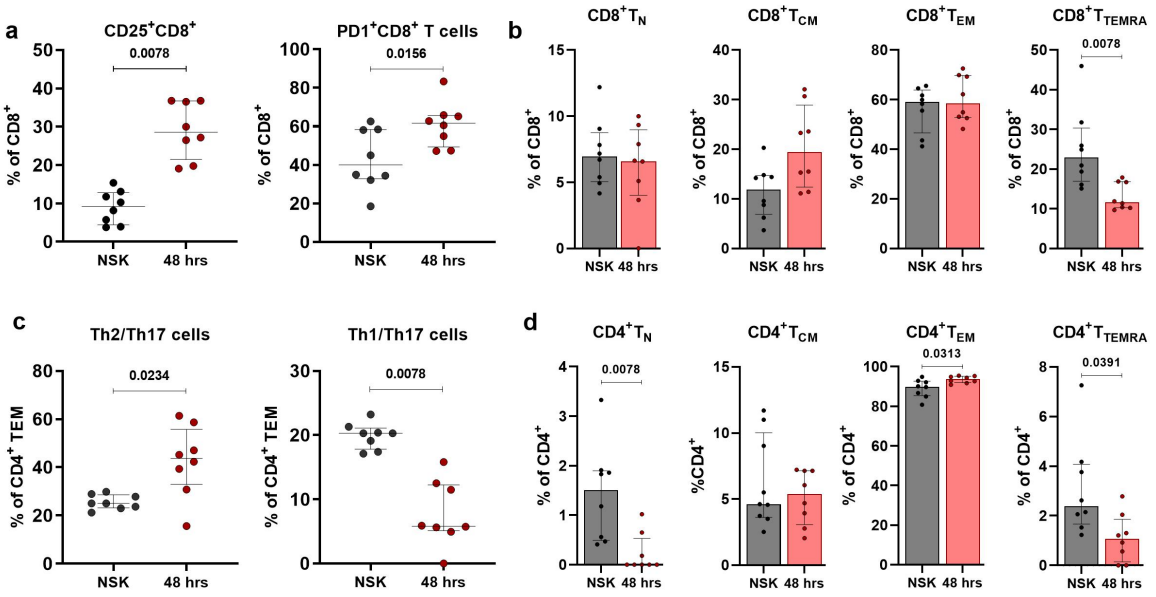


261

262 Figure 5. **Changes in the T cell compartment are observable at 48 hours after mosquito**
263 **exposure. CD8 T cells exhibit a high activation phenotype, while CD4 T effector memory**
264 **cells shift from a Th1/Th17 phenotype to a Th2/Th17 phenotype. a,** Increased frequency of
265 CD25+ and PD1+ CD8 T cells at 48 hours post mosquito exposure. **b,** Frequencies of CD8 T cells
266 naive (CCR7+CD45RA+), central memory (CCR7+CD45RA-), effector memory (CCR7-
267 CD45RA-) and TEMRA (CCR7-CD54RA+) frequencies. **c,** decreased Th1/Th17 and increased
268 Th2/Th17 effector memory CD4 T cell compartment at 48 hours. **d,** CD4 T cells naive
269 (CCR7+CD45RA+), central memory (CCR7+CD45RA-), effector memory (CCR7-CD45RA-)
270 and TEMRA (CCR7-CD54RA+) frequencies. Statistical analysis of 8 samples dedicated to this
271 time point was performed with Wilcoxon signed-rank test. Bars indicate median and interquartile
272 range.

273

274 **"Bitten" human skin cells stimulated by *Aedes aegypti* saliva produce significantly less pro-**
275 **inflammatory cytokines**

276 Next, we sought to assess if *Ae. aegypti* saliva impacted cytokine production by skin cells taken
277 48 hours post-bite. We measured pro- and anti-inflammatory cytokines released into the media
278 after a stimulation assay with and without *Ae. aegypti* SGE. Both NSK and SGE-treated cells
279 showed low secretion of cytokines in the media (Supplementary Figure S9). However, we
280 observed a significant reduction in the levels of Interleukin 2 (IL-2) and Interferon gamma (IFN-
281 γ) in the cells treated with both SGE and PMA/Ionomycin compared to the cells treated with
282 PMA/Ionomycin alone (Fig. 6, Supplementary Figure S9). The levels of other pro-inflammatory
283 cytokines like TNF-α, IL-17A and IL-17F showed no significant differences (Fig. 6). Similarly,
284 no differences in the regulatory cytokine IL-10 was observed (Fig. 6). This data suggests that SGE
285 has a dampening effect on the production of pro-inflammatory cytokines IL-2 and IFN-γ under
286 stimulatory conditions in "bitten" human skin cells.

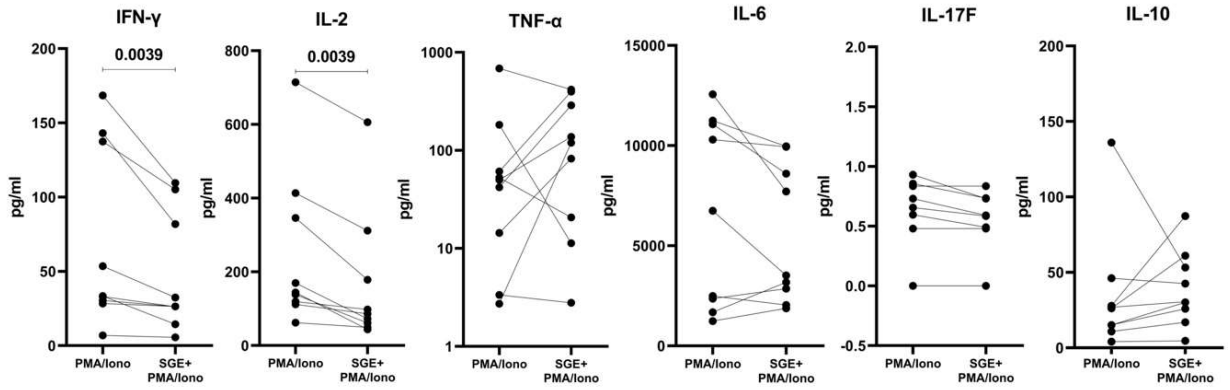


287

288 Figure 6. **Human skin cells obtained from *Ae. aegypti* bitten skin stimulated by *Ae. aegypti***
289 **salivary gland extract (SGE) produce significantly less pro-inflammatory cytokines (IL-2**
290 **and IFN-γ)**. Cytokine production measured in skin cell culture supernatant after treatment with

291 PMA/Ionomycin in the presence or absence of SGE. Skin dissociated cells were seeded on round
292 bottom 96-well plates (50.000 cells/well) and treated with SGE (10 µg/mL) or PBS for 24 hours.
293 Cells were stimulated with PMA (0.1µg/mL) and Ionomycin (1µg/mL) or left unstimulated for the
294 last 6 hours of the culture. Statistical analysis was performed with Wilcoxon signed-rank test. N=9
295 individuals.

296

297 **Discussion**

298 Arboviruses enter the host through the skin when the arthropod injects its saliva and other
299 components into the dermis while taking a bloodmeal. Data from mice and macaques suggest that
300 the unique dual presence of virus and saliva orchestrates an immunological cascade of events that
301 influence the establishment and course of infection[12,16,17]. To translate these findings to humans,
302 the current study assessed the dynamics of the cutaneous immune response to arthropod bites from
303 a clinically relevant vector, the *Ae. aegypti* mosquito, in humans from arboviral-endemic areas
304 with lifelong exposure to *Aedes* mosquitos. At 4 hours post-bite, we observed upregulation of
305 genes involved in neutrophil recruitment and increased frequencies of dendritic cells and M2
306 macrophages. As the immune response progressed over two days, we observed an increased
307 frequency of activated, PD-1+CD8+ T cells, a polarization towards Th2/Th17 CD4+ T-cells, and
308 upregulation of IL-10, IL-4, and IL-13 and IFN-γ related pathways. Interestingly, these human
309 skin cells post-bite produced less pro-inflammatory cytokines when stimulated by Ae. aegypti
310 SGE.

311 A mosquito 'bite' results in minor tissue damage by the proboscis, injection of mosquito saliva
312 into the skin, and introduction of both mosquito and host microbiota into the skin. In this study,

313 we did not parse out the separate impact of each process on the skin immune response. Alterations
314 in skin immunity due to injury from the punch biopsy itself were mitigated by ensuring biopsy
315 sites were at least 10 to 20 mm away from one another and were not taken directly at the site of
316 the needle administration of subcutaneous lidocaine. The effect of local anesthetic was mitigated
317 by the case-control design that each person's anesthetized, bitten skin was compared to
318 anesthetized, unbitten skin, presumably negating any immediate cutaneous immune effects
319 attributed to lidocaine, for which the literature is sparse.

320 Mosquito bites cause a local cutaneous reaction with wheal and flare manifestation[20,21].
321 Concordantly, the bite size reaction peaked after 15 minutes post-bite in this endemic study
322 population. Few changes were detected in gene expression or influx and activation of neutrophils,
323 dendritic cells subsets and macrophages at the 30 minutes post-bite time point. Upregulated genes
324 were related to top-level processes such as signal transduction. We did not design this study to
325 assess the role of pre-stored immune mediators such as histamine (and others) in the development
326 of edema and their modulation in the immune response. Indeed, mosquito bites can activate
327 cutaneous mast cells, which are prominent histamine-storing cells, and induce their degranulation.
328 The release of histamine and other mediators leads to vasodilation, fluid accumulation at the bite
329 site, and neutrophil influx, which were all ultimately observed here[20,21].

330 As the immune reaction progressed, the mosquito 'bite' induced degradation of the extracellular
331 matrix (ECM), and a strong influx of dendritic cells and macrophages at 4 hours post-bite,
332 consistent with previous animal observations[22]. We observed several disintegrin and
333 metalloprotease with thrombospondin type I motifs (ADAMTS) were upregulated, mostly at 4
334 hours post-bite, that can be associated with ECM degradation. Similarly, granzyme B (GZMB)
335 upregulated at 48 hours, despite its effects on inducing inflammation it may also be involved in

336 ECM degradation using as substrate fibronectin, vitronectin, laminin and others[23,24]. Saliva from
337 blood-feeding arthropods contains anti-hemostatic proteins that prevent coagulation and promote
338 vasodilation, leading to increased leukocyte trafficking[20,25]. These processes – extracellular matrix
339 degradation and vasodilation – can facilitate viral infection by disrupting vascular functions, as is
340 the case of sialokinin, a mosquito salivary protein that hinders endothelial barrier integrity[26]. In
341 addition, elevated leukocyte trafficking can facilitate viral replication by augmenting the
342 proportion of susceptible cells to the local inoculation site[12,15,26]. Indeed, as most leukocyte subsets
343 are permissive to infection by most arboviruses, they play a dual role in the infection process: both
344 as replication targets/dissemination vehicles and as the first line of defense. Indeed, the increased
345 presence of activated M2 macrophages and dendritic cells at 4 hours post-bite highlight the cellular
346 trafficking role initiated by 'the bite' that can ultimately result in viral dissemination. The observed
347 increase in CD163+CD14+ cells at 4 hours is what we believe to be an initiation of the
348 differentiation of monocytes and macrophages into M2-skewed macrophages given that full
349 macrophage polarization does not occur as early as 4 hours [27–29]. Upregulated chemokines such as
350 CCL2 and CCL7, attracting mainly monocytes, DCs and T cell, may be participating in this
351 recruitment[30]. M2-polarized macrophages produce anti-inflammatory cytokines, mediate wound
352 healing processes, and support Th2 responses [31]. Moreover, activation of M2 macrophages
353 positively correlated with the bite size in our study. Upon stimulation, DCs upregulated CD69,
354 preventing them from exiting the tissue and improving the likelihood of antigen internalization.
355 Subsequent CD69 downregulation promotes Sphingosine-1-Phosphate (S1P1) leading to DC
356 migration to the lymph nodes[32]. The CD69-S1P1 mechanism of cell retention in tissue is also well-
357 described for resident T cells,[33] whose role in saliva-mediated immunity is not yet known.

358 *Ae. aegypti* mosquito saliva has a clear impact on neutrophil influx and degranulation. Two
359 recently identified *Ae. aegypti* salivary proteins (NeSt1 and AgBr1) that attract and stimulate
360 neutrophils at the 'bite site,' changing the immune microenvironment and leading to increased
361 early ZIKV replication and enhanced pathogenesis[14,15]. Here, at 4 hours post-bite, chemokines
362 CXCL2, CXCL3, CXCL5, and especially CXCL8, plus the cytokine IL-1B were upregulated
363 returning to levels comparable to NSK at 48 hours post-bite. CXCL2-5 chemokines are responsible
364 for attracting neutrophils and exhibiting angiogenic properties[34]. Pro-inflammatory responses
365 through inflammasome activation and IL-1B production can trigger a sustained neutrophilic
366 response[12]. Microbiota egested during infected sand fly bites contributed to IL-1B production[35],
367 but we were unable to assess the effects attributed to vector microbiota in this study. On the other
368 hand, IL-20 was upregulated at 4 hours post-bite. IL-20 is most active at epithelial sites
369 downregulating IL-1B resulting in deactivation of neutrophil functions such as phagocytosis,
370 granule exocytosis, and migration[36,37]. Increased gene expression for neutrophil recruitment and
371 degranulation at 4 hours post-bite in our Cambodian study population further supports the timing
372 of neutrophil influx seen 3 hours post-bite in bite-experienced C57BL/6 immunocompetent mice[12].
373 How the timing of neutrophil influx would differ in a bite-naïve population is a question that
374 remains to be answered as none of the participants would be considered naïve. Moreover, studies
375 of 'infected bites' would clarify the role of both 'neutrophil influx' and extracellular matrix
376 degradation in facilitating pathogen establishment[12,38], but currently approved human challenge
377 models deliver DENV via needle inoculation, not via mosquito bite[39].

378 As the immune response transitioned from innate to adaptive, a strong T-cell signature emerged at
379 4 and 48 hours emerged after the mosquito 'bite'. CD8+ T cell activation was confirmed by
380 increased expression of CD25, an early activation marker. Skin CD8+ T cells also upregulate PD-

381 1 expression, an immune-checkpoint receptor that is induced by yet can also inhibit T cell
382 activation. PD-1 primarily inhibits effector function acquisition by T cells, the loss of sensitivity
383 after T cell receptor signaling and modulation of cytotoxicity, and inhibition of TNF-α and IL-2
384 production along with T-cell expansion[40,41]. Interestingly, highly activated CD8+ cells have been
385 observed in skin from dengue shock syndrome patients[42,43]. Here at 4 and 48 hours post-bite, CD4+
386 T cells had a skewed phenotype to Th2-like cells and IL-10, IL-13, and IL-4 related pathways were
387 upregulated compared to NSK. CCL18, upregulated at 48 hours post-bite, can be expressed by M2
388 macrophages and is linked to increased IL-4, IL-10, and IL-13, especially in the presence of
389 histamine[44]. Indeed, initial animal experiments also pointed to a Th2-mediated allergic
390 inflammatory response following mosquito bites or inoculation with SGE[13]. In case of arbovirus
391 infection, virus will replicate locally in the skin, and the local skin immune responses will direct
392 the course of the systemic host immune response. At 48 hours post-bite, arboviruses will also have
393 disseminated to draining lymph nodes[45]; hence , the contribution of the localized Th2 polarization
394 at this time point on disease outcome remains to be determined.

395 At 48 hours post-bite, other upregulated genes such as CD28, ICOS, and CTLA-4 further suggest
396 a regulatory role of the CD4+ compartment in controlling the local immune responses to *Ae.*
397 *aegypti* saliva. Th2 polarization is essential to avoid excessive collateral damage from an
398 exacerbated pro-inflammatory response, especially in a situation where the skin immune cells are
399 repeatedly exposed to the same type of insult, as is the case with individuals living in tropical areas
400 of mosquito abundance. Blood DC antigen-2 (CLEC4C), upregulated at 48h compared to NSK, is
401 thought to signal through BDCA-2 to inhibit activation of the NF-κB pathway, inhibit production
402 of type I IFNs, and block TRAIL-mediated cytotoxic activity[46]. This may represent a possible
403 mechanism that differentiates chronically exposed individuals compared to naïve individuals.

404 To consider other potential mechanisms that immunomodulate the microenvironment, we noted
405 increased expression at 48 hours post-bite of ficolin-1 (FCN1), a complement lectin pathway
406 protein that may bind and opsonize mosquito microbiota or salivary components, then activate the
407 complement pathway[47]. Another C-type lectin receptor LSECtin (CLEC4G, increased at 48 hours
408 compared to NSK) negatively regulates T cell-mediated immunity and may be also linked to
409 apoptotic cell clearance by macrophages[48]. Of note, the upregulation of CXCL10 chemokine and
410 its receptor CXCR3 are linked to their major roles of inflammatory reactions, T cell migration, and
411 IFN-γ in the saliva-mediated process[49]. Besides chemokines, the top expressed molecule was an
412 antimicrobial peptide hBD-2 (DEFB4A), produced by neutrophils and keratinocytes. DEFB4A is
413 a marker of inflammation absent in normal skin and responsible for recruitment of memory T cells,
414 immature DCs, mast cells and neutrophils[50,51].

415 In this study, the presence of mosquito saliva inhibited pro-inflammatory cytokine production by
416 'bitten' human skin cells after *in vitro* re-stimulation with SGE. One consideration is that we used
417 SGE, rather than mosquito saliva as forced salivation did not provide sufficient material, but our
418 preparations minimize the cellular components of the salivary glands. The cytokine-dampening
419 effect may partly result from the interaction between salivary components and key checkpoints on
420 different signaling pathways. One example includes the salivary protein LTRIN known to interfere
421 with the Nf-kB pathway by binding to LTβR, thus hindering its dimerization and leading to
422 decreased production of inflammatory cytokines[11]. On the other hand, skin immune tolerance to
423 constant mosquito exposure may also explain the reducing effect of SGE on cytokine production
424 as seen here in our bite-experienced participants[12,19,52].

425 Our results refine and extend the knowledge obtained from mouse models of mosquito biting. For
426 example, in mouse models, increased frequencies of dendritic cells, total macrophages and

427 neutrophils have been detected after mosquito bites [21,53,54]. In our human participants, we also
428 observe an increase in the frequency of these cells, indicating that the mouse models of mosquito
429 biting recapitulate the early innate events in human skin. However, we expand these data by
430 showing that the observed increased frequencies are due to increases in M2-like macrophages,
431 which are activated, and increases in Langerhans cells at 4 hours post-bite in our human
432 participants. Additionally, we substantially increased our knowledge on human T cell responses
433 to mosquito saliva by observing CD8 T cells exhibiting a high activation phenotype, while CD4 T
434 effector memory cells shift from a Th1/Th17 phenotype to a Th2/Th17 phenotype 48 hours post-
435 bite. Saliva or salivary proteins from ticks and sand flies have shown ability to inhibit proliferation
436 of both murine and human cells.[55,56] We here confirm the inhibitory effects of SGE to skin cells
437 recruited during a mosquito bite. Nevertheless, as previously showed in individuals from an
438 endemic area of leishmaniasis,[57] the immune responses to saliva of arthropods also triggers a pro-
439 inflammatory response highlighted by the upregulation of pathways related to interferon genes.
440 This mix of anti- and pro-inflammatory responses need to be further evaluated in animal models
441 of mosquito bite exposure as well as clinical field settings.

442 With the current rise of vector-borne diseases around the world, future clinical development of
443 vector-targeted strategies for both known and unknow vector-borne diseases will require a
444 fundamental understanding of how vector saliva modulates the cutaneous immune response of
445 humans. Translational studies, such as the one presented here, significantly expand our current
446 knowledge on human skin immunity and the immune response orchestrated by a 'mosquito bite'.
447 These newly identified genes, cell types, and processes of human cutaneous immunity can be
448 leveraged in the development of vector-targeted vaccine candidates or novel therapeutics such as
449 those targeting the reversibility of functional macrophage polarization or chemokine blockades

450 that may have application in other inflammatory disorders[58]com. Such new pathogen-agnostic
451 strategies have shown promising results in recent years from mosquito saliva-based vaccinations
452 to topical applications like imiquimod post-bite that activated skin macrophages in order to limit
453 pan-viral activity[59–62]. Building on these findings, the next generation of countermeasures against
454 vector-borne disease will require nuanced and comprehensive understanding of skin immunity to
455 both pathogen and vector saliva alike.

456

457 **Materials and methods**

458 **Study Enrollment and Procedures**

459 From October 2020 to January 2021, we enrolled thirty Cambodian adults at Kampong Speu
460 District Referral Hospital. Eligible participants were healthy adults between the ages of 18 and 45
461 years old who agreed not to use topical or oral antihistamines or steroids for the duration of the
462 study. Participants were excluded if they were pregnant or reported a history of severe allergic
463 reaction to mosquito or other insect bites, use of medications that affect blood clotting, or history
464 of significant scarring such as keloid formation (full criteria found on
465 https://clinicaltrials.gov/ct2/show/NCT04350905). All participants provided written informed
466 consent before enrollment, and the study was conducted in accordance with the provisions of the
467 Declaration of Helsinki and Good Clinical Practice guidelines.

468 On Day 0, five starved uninfected *Ae. aegypti* female mosquitos were selected from a mosquito
469 colony dedicated to human feeding studies in the Malaria and Vector Research Laboratory at the
470 National Center for Parasitology, Entomology and Malaria Control. Mosquitos fed through the
471 disposable mesh of a feeding device placed on participants' ventral forearm skin for 10 minutes.
472 Redness and swelling in millimeters were assessed immediately, 15 minutes, 30 minutes, 4 hours

473 and 48 hours after feeding. Redness and swelling were measured in millimeters at 15 minutes, 30
474 minutes, and 4 hours.

475 A total of five 3-mm skin punch biopsies were performed on each individual: one biopsy from
476 bitten skin per time point (30 minutes, 4 hours, and about 48 hours after feeding is completed) for
477 a total of three 'bitten' biopsies, and two from NSK collected at baseline. Biopsy sites were
478 selected based on the 3 bite sites with the largest diameters at 30 minutes after feeding. We tattooed
479 the area surrounding those 3 bite sites with a permanent marker and randomly picked one of the
480 three distinct sites for 30 min, 4 hours and 48 hours biopsies. Less than 1cc of 0. 2% lidocaine
481 without epinephrine was delivered via 30-G needle each chosen 'bite' at the time of biopsy and 3-
482 mm biopsy was performed on 'bite' adjacent to needle puncture. For feasibility of skin sample
483 analysis, each participant was assigned to 1 of 3 technical modality cohorts: 1)
484 immunohistochemistry, 2) RNASeq, and 3) flow cytometry with ten people in each cohort.
485 Additionally, blood was collected for serological and cellular analyses at baseline and 14 days
486 after feeding.

487 ***Aedes aegypti* SGE preparation**

488 Salivary glands from *Ae. aegypti* were dissected and collected in 200µl of PBS 1x (1pairs/1µl of
489 PBS 1x) in Low protein binding centrifuge tubes. Homogenization was done in an Ultrasonic
490 SONIFIER® (BRANSON) for 30 seconds on each side of the tube. The homogenates were then
491 centrifuged at 25,000 × g at 4 °C for 3 minutes, and the supernatant was collected and quantified
492 using Pierce™ BCA Protein Assay Kit (ThermoFisher Scientific, Cat# 23225) in an xMark™
493 Microplate Spectrophotometer (BIO-RAD).

494 ***Aedes aegypti* salivary IgG enzyme-linked immunosorbent assays**

495 *Ae. aegypti* SGE was diluted to a concentration of 2 ug/ul in carbonate-bicarbonate buffer
496 (Millipore-Sigma) and used to coat 96-well Immulon 4x HB plates (Nunc) overnight at 4°C. Plates
497 were blocked in a solution of TBS 4 % Bovine serum albumin 0.025 % Tween 20 (Millipore-
498 Sigma). Each plate included sera (1:200 dilution) from all time points, a negative control (non-
499 reactive human sera to SGE), an internal control (a pool of positive sera to SGE with OD set to
500 0.25 at 450nm) and blank wells. The controls were chosen accordingly from a stored bank of
501 human sera, well-characterized by reactivity to the saliva of various vectors, at the Laboratory of
502 Malaria and Vector Research. Plate-to-plate normalization was done by multiplication of all OD
503 values by a correcting factor to achieve the preset internal control OD 0.25 at 450nm. Secondary
504 antibody [goat anti-human IgG alkaline phosphatase (1:10000 in blocking solution; Millipore-
505 Sigma). A solution of p-nitrophenylphosphate (Millipore-Sigma) was used as substrate and OD
506 measured at 450nm in arbitrary enzyme-linked immunosorbent assay (ELISA) units and reported
507 in arbitrary ELISA units after correction stated above.

508 **Dengue IgG enzyme-linked immunosorbent assays**

509 The PanBio® Dengue Indirect IgG ELISA (product code 01PE30) was performed according to
510 the manufacturer's instructions. Two microtiter plates were supplied, one containing stabilized
511 dengue-1 through dengue-4 (antigen plate) and the other containing either anti-human IgM or anti-
512 human IgG bound to separate wells (assay plate). Peroxidase-labeled anti-dengue virus
513 monoclonal antibody (125 µl/well) was added to the antigen plate to solubilize the antigens and
514 form antibody-antigen complexes. Concurrently, 100 µl of patient serum was diluted 1:100 in the
515 provided diluent and added to each well of the assay plate containing either bound anti-human IgM
516 or bound anti-human IgG, and human IgM or IgG in the patient's serum was captured. The plates
517 were incubated for 1 h at room temperature (antigen plate) or 37°C (assay plate); then the assay

518 plate was washed, and 100 µl of antibody-antigen complexes per well was transferred from the
519 antigen plate to the assay plate. These complexes were captured by dengue virus-specific IgM or
520 IgG during incubation for 1 h at 37°C. The plate was washed, and bound complexes were
521 visualized through the addition of 100 µl of tetramethylbenzidine substrate per well. After 10 min,
522 the reaction was stopped by the addition of 100 µl of 1 M phosphoric acid per well, and the strips
523 were read at 450 nm with a microtiter plate reader. Positivity was determined by comparison to
524 the IgM and IgG reference sera provided (cutoff calibrators). A positive sample was defined as
525 having a sample/calibrator absorbance ratio of ≥1.0, and a negative sample was defined as having
526 a ratio of <1.0.

527 **Formalin preservation and H&E staining of skin biopsies**

528 Biopsies were placed in 7ml prefilled 10% formalin vials (Azer Scientific) and stored at 4°C until
529 paraffin embedded. Unstained slides were cut from paraffin blocks and deparaffinized in xylene,
530 then hydrated through graded alcohols up to water, placed in Carazzi's hematoxylin, washed in
531 tap water, and put in one change 95% ethanol. Next, they were placed in eosin-phloxine solution
532 and then run through graded alcohols to xylene. After xylene, the stained slides were than a cover
533 slip was mounted using Permount Mounting Media (Fisher Scientific).

534 **RNA extraction, RNA-seq library preparation, sequencing and analysis.**

535 Biopsies were stored in DNA/RNA Shield (Zymo research) and kept in 4 °C until processing. Skin
536 was homogenized using 3mm zirconium beads (Biolink laboratories) and a Magnalyser bead
537 beater (Roche Diagnostics®). After homogenization total RNA was loaded at InnuPure® C16
538 touch (AnalitikJena) for magnetic separation of total RNA using an InnuPREP® RNA Kit–IPC16
539 (AnalitikJena). Quality of extractions was verified on a 4200 TapeStation (Agilent) and all samples
540 had RIN numbers above seven. RNA sequencing was performed by Novogene. Briefly, mRNA

541 was enriched by Poly (A) capture and RNA libraries were prepared using the NEBNext Ultra II
542 Directional RNA Library Prep Kit for Illumina (New England Biolabs) and sequenced on a
543 NovaSeq 6000 (Illumina) generating paired end reads at 150 bp length. After removing low quality
544 reads (Trimommatic 0.39)[63], mapping to the human genome (hg38; GCF_000001405.39) and
545 gene-level quantification were generated by RSEM 1.3.2[64], Bowtie 2-2.4.2[65] and SAMtools
546 1.11[66]. Normalization and differential gene expression (DGE) analysis were performed using
547 DESeq2 1.34.0[67], employing the variance stabilizing transformed function (VSN 3.62.0)[68] to the
548 count matrix, that was designed to account for paired samples enabling expression analyses with
549 normal skin samples from the same subject as reference. Approximate Posterior Estimation for
550 GLM (Apeglm 1.16.0) method was used to calculate fold change of DEGs[69]. DEGs were
551 considered significant if apeglm-estimated shrunken log2fold change was <1 or >1 and with a false
552 discovery rate <0.05 (Benjamini–Hochberg multiple testing correction method[70]). PlotPCA3D
553 0.0.1(twbattaglia/btools) was used to generate tri-dimensional principal component analysis plots
554 on DESeq2. EnhancedVolcano 1.12.0 was used to generate volcano plots[71]. GOplot 1.0.[72] was
555 used to generate chord plots using data obtained from packages clusterProfiler 4.2.0[73] and
556 ReactomePA 1.38.0[74]. Pathways with a Benjamini–Hochberg corrected P value <0.05 and were
557 considered as enriched, selected pathways were mapped on chord plots[70]. Heatmaps were prepared
558 using package pheatmap 1.0.12.[75] and dendsort 0.3.4[76]. All DEG analyses were performed using
559 R 4.1.0[77].

560 **Skin biopsy dissociation**

561 Biopsies were transported in RPMI media (Sigma-Aldrich) at 4 °C. Whole skin dissociation kit
562 (Miltenyi®) was used to perform the biopsies dissociation. An enzyme mix consisting of enzyme
563 D, enzyme A and buffer L was prepared according to the manufacturer's specifications. Single

564 punch biopsies were incubated in 400 µl of dissociation mix, at 37°C – 5% CO2 overnight.
565 Following incubation, each sample mix was transferred to a Falcon round-bottom tube with cell-
566 strainer cap (40-75um). Using a rubber pestle and the cell-strainer cap as a mortar, biopsies where
567 gently macerated to increase cell recovery yield. 500 µl of cold RMPI was used to rinse caps.
568 Samples were then centrifuged at 1500 rpm 4°C for 10 minutes and the pellet resuspended in 500
569 µl of cold RPMI. Dissociated skin cells were counted using a pre-programmed setting in a
570 Countess™ II FL Automated Cell Counter.

571 **Flow cytometry**

572 Dissociated cells were seeded on round bottom 96-well plates and washed with 200 µl of
573 ThermoFisher's PBS buffer 1x (1500 rpm, 4°C for 5 minutes). Twenty µl of Biolegend Zombie
574 Aqua fixable viability stain (1:500) was added and incubated for 20 minutes in the dark at 4°C.
575 Excess viability stain was washed away with 200 µl of PBS/BSA/EDTA buffer (1500 rpm, 4°C
576 for 5 minutes), and the pellet resuspended and incubated for 10 minutes at 4°C in 4 µl of
577 Biolegend's FcR blocking antibody (1:10). Cells were then incubated for 30 minutes at 4°C with
578 surface staining antibody master mix. After washing free unbound antibody with 200 µl of PBS
579 (1500 rpm, 4°C for 5 minutes), cells were fixed with 100 µl of Biolegend's fixation buffer 1x for
580 20 minutes at 4°C in the dark. Following fixation, cells were permeabilized and washed with 100
581 µl of Biolegend perm-wash solution 1x (1500 rpm, 4°C for 5 minutes) and the pellet resuspended
582 and incubated for 30 minutes at 4°C in intracellular staining antibody master mix. Stained cells
583 were placed in 200 µl of PBS/BSA/EDTA 1x and visualized on a BD Biosciences FACS Aria II
584 using FACS Diva software. Analysis was performed using BD Biosciences FlowJo software.
585 Antibody panels are described in supplemental material (Supplementary Table 5).

586 **In vitro SGE stimulation and Multiplex cytokine screening**

587 Skin dissociated cells were seeded on round bottom 96-well plates (50.000 cells/well) and treated
588 with SGE (10 µg/mL) or PBS for 24 hours. Cells were stimulated with PMA (0.1µg/mL) and
589 Ionomycin (1µg/mL) or left unstimulated for the last 6 hours of the culture. The supernatants were
590 collected and stored at -20°C. Cytokines in the cell culture supernatants were quantified using
591 Human Th Cytokine Panel (12-plex) (Cat. 741027, BioLegend) according to the manufacturer's
592 instructions. All samples in the experiment were measured in duplicate. Briefly, undiluted
593 supernatants were incubated with beads coated with capture antibodies specific for IL-2, 4, 5, 6,
594 9, 10, 13, 17A, 17F, 22, IFN-γ and TNF-α for 2 hours at room temperature on shaker. After
595 incubation, beads were washed and incubated with biotin-labeled detection antibodies for 1 hour,
596 followed by a final incubation with streptavidin-PE for 30 minutes at room temperature on shaker.
597 Beads were washed and re-suspended with washing buffer. Beads were analyzed by flow
598 cytometry using a FACS Canto cytometer. Analysis was performed using the LEGENDplex
599 analysis software v8.0, which distinguishes between the 12 different analytes on basis of bead size
600 and internal dye.

601 **Statistical analyses**

602 Flow cytometry and multiplex cytokine screening data were analyzed using the non-parametric-
603 based tests, Wilcoxon signed-rank and Chi-square test. Correlation analysis was performed with
604 the Pearson's correlation coefficient. Bars indicate median and interquartile range, and p-values
605 *$p<0.05$, **$p<0.01$, ***$p<0.001$. Statistical analysis of RNAseq data is described above.

606 **Acknowledgements**

607 We would like to thank the study participants in Kampong Speu, Cambodia. We would also like
608 to acknowledge Noemi Kedei and Maria Hernandez for their assistance in histology and staining
609 as well as Jon Fintzi for statistical review of the clinical protocol.

**Funding**

This work was funded by the Division of Intramural Research at National Institute of Allergy and Infectious Diseases at the National Institutes of Health. T.C. is a HHMI-Wellcome international research scholar (208710/Z/17/Z). D.M is funded by the French National Research Agency (ANR-**17**-CE15-00029) . D.G. is supported by a Calmette-Yersin PhD scholarship funded by the Institute Pasteur International Network.

**Competing interests**

The authors declare no competing interests.

**Author contributions**

Conceptualization: F.O., J.E.M., T.C., J.G.V. Methodology: D.G., H.V, S.N., S.C., S.L., J.A.B., F.O., J.E.M.. Investigation: D.G., H.V, J.A.B, S.N., S.C., S.L., A.P., J.G.V., F.O., J.E.M. Visualization: D.G., F.O., J.A.B. Funding acquisition: F.O., J.E.M. Study enrollment and clinical procedures: C.L, S.L., R.S, S.S., S.N., J.M, H.K, R.L. Project administration: C.L., T.C., F.O., J.E.M., Supervision: T.C., D.M, F.O., J.E.M., C.L, R.L., H.R, H.K. Writing original draft: D.G., H.V., T.C., F.O., J.E.M., J.A.B. Writing review and editing: T.C., D.M., C.L., F.O., J.A.B., J.E.M.

All authors contributed to the article and approved the submitted version

**Data availability**

The Illumina raw reads (fastq files) were loaded at the NCBI Sequence Read Archive with accession numbers SRR18215008 to SRR18215047 and deposited in GenBank under bioproject accession code PRJNA812009. All data generated or analyzed during this study are included in this published article (and its supplementary information files). Clinical trial data is

631 available at https://clinicaltrials.gov/ct2/show/NCT04350905. Flow cytometry data can be made
632 available upon reasonable request directly to the authors.

633 **Bibliography**


634 1. WHO. A global brief on vector-borne diseases. *www.who.int* (2020).
635 2. Pierson, T. C. & Diamond, M. S. The continued threat of emerging flaviviruses. *Nat. Microbiol.* **5**,
636 796–812 (2020).
637 3. Ryan, S. J., Carlson, C. J., Mordecai, E. A. & Johnson, L. R. Global expansion and redistribution of
638 Aedes-borne virus transmission risk with climate change. *PLoS Negl. Trop. Dis.* **13**, e0007213 (2019).
639 4. Godoy, R. S. M. *et al.* Dengue and Zika virus infection patterns vary among Aedes aegypti field
640 populations from Belo Horizonte, a Brazilian endemic city. *PLoS Negl. Trop. Dis.* **15**, e0009839
641 (2021).
642 5. Sun, P. *et al.* A mosquito salivary protein promotes flavivirus transmission by activation of
643 autophagy. *Nat. Commun.* **11**, 260 (2020).
644 6. Ha, Y.-R. *et al.* Detection of Heparin in the Salivary Gland and Midgut of Aedes togoi. *Korean J.*
645 *Parasitol.* **52**, 183–188 (2014).
646 7. Schneider, B. S. & Higgs, S. The enhancement of arbovirus transmission and disease by mosquito
647 saliva is associated with modulation of the host immune response. *Trans. R. Soc. Trop. Med. Hyg.*
648 **102**, 400–408 (2008).
649 8. Guerrero, D., Cantaert, T. & Missé, D. Aedes Mosquito Salivary Components and Their Effect on the
650 Immune Response to Arboviruses. *Front. Cell. Infect. Microbiol.* **10**, 407 (2020).
651 9. Manning, J. E. & Cantaert, T. Time to Micromanage the Pathogen-Host-Vector Interface:
652 Considerations for Vaccine Development. *Vaccines* **7**, 10 (2019).

653 10. Vogt, M. B. *et al.* Mosquito saliva alone has profound effects on the human immune system. *PLoS*
654 *Negl. Trop. Dis.* **12**, e0006439 (2018).
655 11. Jin, L. *et al.* Salivary factor LTRIN from Aedes aegypti facilitates the transmission of Zika virus by
656 interfering with the lymphotoxin-β receptor. *Nat. Immunol.* **19**, 342–353 (2018).
657 12. Pingen, M. *et al.* Host Inflammatory Response to Mosquito Bites Enhances the Severity of Arbovirus
658 Infection. *Immunity* **44**, 1455–1469 (2016).
659 13. Schneider, B. S., Soong, L., Zeidner, N. S. & Higgs, S. Aedes aegypti salivary gland extracts modulate
660 anti-viral and TH1/TH2 cytokine responses to sindbis virus infection. *Viral Immunol.* **17**, 565–573
661 (2004).
662 14. Hastings, A. K. *et al.* Aedes aegypti NeSt1 Protein Enhances Zika Virus Pathogenesis by Activating
663 Neutrophils. *J. Virol.* **93**, e00395-19, /jvi/93/13/JVI.00395-19.atom (2019).
664 15. Uraki, R. *et al.* Aedes aegypti AgBR1 antibodies modulate early Zika virus infection of mice. *Nat.*
665 *Microbiol.* **4**, 948–955 (2019).
666 16. McCracken, M. K. *et al.* Route of inoculation and mosquito vector exposure modulate dengue virus
667 replication kinetics and immune responses in rhesus macaques. *PLoS Negl. Trop. Dis.* **14**, e0008191
668 (2020).
669 17. Dudley, D. M. *et al.* Infection via mosquito bite alters Zika virus tissue tropism and replication
670 kinetics in rhesus macaques. *Nat. Commun.* **8**, 2096 (2017).
671 18. Trager, W. Acquired Immunity to Ticks. *J. Parasitol.* **25**, 57 (1939).
672 19. Guilbride, D. L., Guilbride, P. D. L. & Gawlinski, P. Malaria's deadly secret: a skin stage. *Trends*
673 *Parasitol.* **28**, 142–150 (2012).
674 20. Conway, M. J. Type I hypersensitivity promotes Aedes aegypti blood feeding. *Sci. Rep.* **11**, 14891
675 (2021).

676 21. Demeure, C. E. *et al.* Anopheles Mosquito Bites Activate Cutaneous Mast Cells Leading to a Local
677 Inflammatory Response and Lymph Node Hyperplasia. *J. Immunol.* **174**, 3932–3940 (2005).
678 22. Conway, M. J. *et al.* Mosquito Saliva Serine Protease Enhances Dissemination of Dengue Virus into
679 the Mammalian Host. *J. Virol.* **88**, 164–175 (2014).
680 23. Turner, C. T., Lim, D. & Granville, D. J. Granzyme B in skin inflammation and disease. *Matrix Biol.* **75–**
681 **76**, 126–140 (2019).
682 24. Buzza, M. S. *et al.* Extracellular Matrix Remodeling by Human Granzyme B via Cleavage of
683 Vitronectin, Fibronectin, and Laminin. *J. Biol. Chem.* **280**, 23549–23558 (2005).
684 25. Champagne, D. E. Antihemostatic Molecules from Saliva of Blood-Feeding Arthropods. *Pathophysiol.*
685 *Haemost. Thromb.* **34**, 221–227 (2005).
686 26. Lefteri, D. A. *et al. Mosquito saliva sialokinin-dependent enhancement of arbovirus infection through*
687 *endothelial barrier leakage*. http://biorxiv.org/lookup/doi/10.1101/2021.02.19.431961 (2021)
688 doi:10.1101/2021.02.19.431961.
689 27. Davies, L. C., Jenkins, S. J., Allen, J. E. & Taylor, P. R. Tissue-resident macrophages. *Nat. Immunol.* **14**,
690 986–995 (2013).
691 28. Mantovani, A., Sica, A. & Locati, M. Macrophage Polarization Comes of Age. *Immunity* **23**, 344–346
692 (2005).
693 29. Mantovani, A., Biswas, S. K., Galdiero, M. R., Sica, A. & Locati, M. Macrophage plasticity and
694 polarization in tissue repair and remodelling: Macrophage plasticity and polarization in tissue repair
695 and remodelling. *J. Pathol.* **229**, 176–185 (2013).
696 30. Bardina, S. V. *et al.* Differential Roles of Chemokines CCL2 and CCL7 in Monocytosis and Leukocyte
697 Migration during West Nile Virus Infection. *J. Immunol.* **195**, 4306–4318 (2015).
698 31. Mills, C. D. Anatomy of a Discovery: M1 and M2 Macrophages. *Front. Immunol.* **6**, (2015).

699 32. Lamana, A. *et al.* CD69 Modulates Sphingosine-1-Phosphate-Induced Migration of Skin Dendritic
700 Cells. *J. Invest. Dermatol.* **131**, 1503–1512 (2011).
701 33. Mackay, L. K. *et al.* Cutting Edge: CD69 Interference with Sphingosine-1-Phosphate Receptor
702 Function Regulates Peripheral T Cell Retention. *J. Immunol.* **194**, 2059–2063 (2015).
703 34. Rajarathnam, K., Schnoor, M., Richardson, R. M. & Rajagopal, S. How do chemokines navigate
704 neutrophils to the target site: Dissecting the structural mechanisms and signaling pathways. *Cell.*
705 *Signal.* **54**, 69–80 (2019).
706 35. Dey, R. *et al.* Gut Microbes Egested during Bites of Infected Sand Flies Augment Severity of
707 Leishmaniasis via Inflammasome-Derived IL-1β. *Cell Host Microbe* **23**, 134-143.e6 (2018).
708 36. Gough, P., Ganesan, S. & Datta, S. K. IL-20 Signaling in Activated Human Neutrophils Inhibits
709 Neutrophil Migration and Function. *J. Immunol.* **198**, 4373–4382 (2017).
710 37. Myles, I. A. *et al.* Signaling via the IL-20 receptor inhibits cutaneous production of IL-1β and IL-17A
711 to promote infection with methicillin-resistant Staphylococcus aureus. *Nat. Immunol.* **14**, 804–811
712 (2013).
713 38. Lefteri, D. A. *et al.* Mosquito saliva enhances virus infection through sialokinin-dependent vascular
714 leakage. *Proc. Natl. Acad. Sci.* **119**, e2114309119 (2022).
715 39. Kirkpatrick, B. D. *et al.* The live attenuated dengue vaccine TV003 elicits complete protection against
716 dengue in a human challenge model. *Sci. Transl. Med.* **8**, (2016).
717 40. Shimizu, K. *et al.* PD-1 Imposes Qualitative Control of Cellular Transcriptomes in Response to T Cell
718 Activation. *Mol. Cell* **77**, 937-950.e6 (2020).
719 41. Wei, F. *et al.* Strength of PD-1 signaling differentially affects T-cell effector functions. *Proc. Natl.*
720 *Acad. Sci.* **110**, E2480–E2489 (2013).
721 42. Duyen, H. T. L. *et al.* Skin dendritic cell and T cell activation associated with dengue shock syndrome.
722 *Sci. Rep.* **7**, 14224 (2017).

723 43. Rivino, L. *et al.* Virus-specific T lymphocytes home to the skin during natural dengue infection. *Sci.*
724 *Transl. Med.* **7**, (2015).
725 44. Mommert, S., Schaper, J. T., Schaper-Gerhardt, K., Gutzmer, R. & Werfel, T. Histamine Increases Th2
726 Cytokine-Induced CCL18 Expression in Human M2 Macrophages. *Int. J. Mol. Sci.* **22**, 11648 (2021).
727 45. Styer, L. M. *et al.* Mosquito Saliva Causes Enhancement of West Nile Virus Infection in Mice. *J. Virol.*
728 **85**, 1517–1527 (2011).
729 46. Chiffoleau, E. C-Type Lectin-Like Receptors As Emerging Orchestrators of Sterile Inflammation
730 Represent Potential Therapeutic Targets. *Front. Immunol.* **9**, 227 (2018).
731 47. Holmskov, U., Thiel, S. & Jensenius, J. C. Collectins and Ficolins: Humoral Lectins of the Innate
732 Immune Defense. *Annu. Rev. Immunol.* **21**, 547–578 (2003).
733 48. Tang, L. *et al.* Liver Sinusoidal Endothelial Cell Lectin, LSECtin, Negatively Regulates Hepatic T-Cell
734 Immune Response. *Gastroenterology* **137**, 1498-1508.e5 (2009).
735 49. Kuo, P. T. *et al.* The Role of CXCR3 and Its Chemokine Ligands in Skin Disease and Cancer. *Front.*
736 *Med.* **5**, 271 (2018).
737 50. Niyonsaba, F., Ogawa, H. & Nagaoka, I. Human beta-defensin-2 functions as a chemotactic agent for
738 tumour necrosis factor-alpha-treated human neutrophils. *Immunology* **111**, 273–281 (2004).
739 51. Niyonsaba, F., Iwabuchi, K., Matsuda, H., Ogawa, H. & Nagaoka, I. Epithelial cell-derived human β-
740 defensin-2 acts as a chemotaxin for mast cells through a pertussis toxin-sensitive and phospholipase
741 C-dependent pathway. *Int. Immunol.* **14**, 421–426 (2002).
742 52. Rizzo, C. *et al.* IgG1 and IgG4 Antibody Responses to the Anopheles gambiae Salivary Protein gSG6 in
743 the Sympatric Ethnic Groups Mossi and Fulani in a Malaria Hyperhendemic Area of Burkina Faso.
744 *PLoS ONE* **9**, e96130 (2014).
745 53. McKimmie, C. S., Pingen, M., Bryden, S. R. & Lefteri, D. A. Host inflammatory response to mosquito
746 bites enhances the severity of arbovirus infection. *ISBT Sci. Ser.* **13**, 76–79 (2018).

747 54. Henrique, M. O. *et al.* Evaluation of inflammatory skin infiltrate following *Aedes aegypti* bites in
748 sensitized and non-sensitized mice reveals saliva-dependent and immune-dependent phenotypes.
749 *Immunology* **158**, 47–59 (2019).
750 55. Qureshi, A. A. *et al.* Immunomodulatory properties of maxadilan, the vasodilator peptide from sand
751 fly salivary gland extracts. *Am. J. Trop. Med. Hyg.* **54**, 665–671 (1996).
752 56. Gillespie, R. D., Dolan, M. C., Piesman, J. & Titus, R. G. Identification of an IL-2 binding protein in the
753 saliva of the Lyme disease vector tick, Ixodes scapularis. *J. Immunol. Baltim. Md 1950* **166**, 4319–
754 4326 (2001).
755 57. Oliveira, F. *et al.* Delayed-Type Hypersensitivity to Sand Fly Saliva in Humans from a Leishmaniasis-
756 Endemic Area of Mali Is TH1-Mediated and Persists to Midlife. *J. Invest. Dermatol.* **133**, 452–459
757 (2013).
758 58. Pasparakis, M., Haase, I. & Nestle, F. O. Mechanisms regulating skin immunity and inflammation.
759 *Nat. Rev. Immunol.* **14**, 289–301 (2014).
760 59. Manning, J. E. *et al.* Safety and immunogenicity of a mosquito saliva peptide-based vaccine: a
761 randomised, placebo-controlled, double-blind, phase 1 trial. *The Lancet* S0140673620310485 (2020)
762 doi:10.1016/S0140-6736(20)31048-5.
763 60. Oliveira, F. *et al.* A sand fly salivary protein vaccine shows efficacy against vector-transmitted
764 cutaneous leishmaniasis in nonhuman primates. *Sci. Transl. Med.* **7**, (2015).
765 61. Sajid, A. *et al.* mRNA vaccination induces tick resistance and prevents transmission of the Lyme
766 disease agent. *Sci. Transl. Med.* **13**, eabj9827 (2021).
767 62. Bryden, S. R. *et al.* Pan-viral protection against arboviruses by activating skin macrophages at the
768 inoculation site. *Sci. Transl. Med.* **12**, eaax2421 (2020).
769 63. Bolger, A. M., Lohse, M. & Usadel, B. Trimmomatic: a flexible trimmer for Illumina sequence data.
770 *Bioinformatics* **30**, 2114–2120 (2014).

771 64. Li, B. & Dewey, C. N. RSEM: accurate transcript quantification from RNA-Seq data with or without a
772 reference genome. *BMC Bioinformatics* **12**, 323 (2011).
773 65. Langmead, B. & Salzberg, S. L. Fast gapped-read alignment with Bowtie 2. *Nat. Methods* **9**, 357–359
774 (2012).
775 66. Dobin, A. & Gingeras, T. R. Mapping RNA-seq Reads with STAR. *Curr. Protoc. Bioinforma.* **51**, (2015).
776 67. Love, M. I., Huber, W. & Anders, S. Moderated estimation of fold change and dispersion for RNA-seq
777 data with DESeq2. *Genome Biol.* **15**, 550 (2014).
778 68. Huber, W., von Heydebreck, A., Sultmann, H., Poustka, A. & Vingron, M. Variance stabilization
779 applied to microarray data calibration and to the quantification of differential expression.
780 *Bioinformatics* **18**, S96–S104 (2002).
781 69. Zhu, A., Ibrahim, J. G. & Love, M. I. Heavy-tailed prior distributions for sequence count data:
782 removing the noise and preserving large differences. *Bioinformatics* **35**, 2084–2092 (2019).
783 70. Benjamini, Y. & Hochberg, Y. Controlling the False Discovery Rate: A Practical and Powerful
784 Approach to Multiple Testing. *J. R. Stat. Soc. Ser. B Methodol.* **57**, 289–300 (1995).
785 71. Blighe, K., Rana, S. & Lewis, M. Enhanced Volcano: publication-ready volcano plots with enhanced
786 colouring and labeling. (2021).
787 72. Walter, W., Sánchez-Cabo, F. & Ricote, M. GOplot: an R package for visually combining expression
788 data with functional analysis: Fig. 1. *Bioinformatics* **31**, 2912–2914 (2015).
789 73. Yu, G., Wang, L.-G., Han, Y. & He, Q.-Y. clusterProfiler: an R Package for Comparing Biological
790 Themes Among Gene Clusters. *OMICS J. Integr. Biol.* **16**, 284–287 (2012).
791 74. Yu, G. & He, Q.-Y. ReactomePA: an R/Bioconductor package for reactome pathway analysis and
792 visualization. *Mol. Biosyst.* **12**, 477–479 (2016).
793 75. Kolde, R. Pretty Heatmaps. R package version.

76. Sakai, R., Winand, R., Verbeiren, T., Moere, A. V. & Aerts, J. dendsort: modular leaf ordering methods for dendrogram representations in R. *F1000Research* **3**, 177 (2014).

77. R Core Team (2021). *R: A language and environment for statistical computing. R Foundation fo Statistical Computing, Vienna, Austria*. (The R Foundation).